Comparison study on the ammonium adsorption of the biochars derived from different kinds of fruit peel

Xiaojian Hu[a,b,1], Xinbo Zhang[a,b,1], Huu Hao Ngo[a,c,*], Wenshan Guo[a,c], Haitao Wen[a,b], Chaocan Li[a,b], Yongchao Zhang[a,b], Chanjuan Ma [a,b]

[a] *Joint Research Centre for Protective Infrastructure Technology and Environmental Green Bioprocess, Department of Environmental and Municipal Engineering, Tianjin Chengjian University, Tianjin 300384, China and School of Civil and Environmental Engineering, University of Technology Sydney, NSW 2007, Australia*

[b] *Tianjin Key Laboratory of Aquatic Science and Technology, Tianjin Chengjian University, Jinjing Road 26, Tianjin 300384, China*

[c] *Centre for Technology in Water and Wastewater, School of Civil and Environmental Engineering, University of Technology Sydney, Sydney, NSW 2007, Australia*

[1]*Equal contribution*

*Correspondence author. Email address: ngohuuhao121@gmail.com

Abstract

Application of biochars to remove inorganic nitrogen (NH_4^+、NO_2^-、NH_3、NO、NO_2、N_2O) from wastewater and agricultural fields has gained a significant interest. This study aims to investigate the relationship between ammonium sorption and physicochemical properties of biochars derived from different kinds of fruit peel. Biochars from three species of fruit peel (orange, pineapple and pitaya) were prepared at 300, 400, 500 and 600℃ with the residence time of 2h and 4h. Their characteristics and sorption for ammonium was evaluated. The results show a clear effect of pyrolysis conditions on physicochemical properties of biochars, including elemental composition, functional groups and pH. The maximum NH_4^+ adsorption capacities were associated with biochars of orange peel (4.71mg/g) and pineapple peel (5.60mg/g) produced at 300 ℃ for 2h. The maximum NH_4^+ adsorption capacity of the pitaya peel biochar produced at 400 ℃ for 2h was 2.65mg/g. For all feedstocks, biochars produced at low temperatures showed better NH_4^+ adsorption capacity. It was found that biochars had better adsorption efficiency on ammonium at a pH of 9. Adsorption kinetics of ammonium on biochars followed the pseudo-second-order kinetic model whilst Langmuir isotherm model could well simulate the adsorption behavior of ammonium on biochars. The adsorption mechanism of ammonium on biochars predominantly involved surface complexation, cation exchange and electrostatic attraction**.** Conclusively, the fruit peel-derived biochars can be used as an alternative to conventional sorbents in water treatment.

Key words: Fruit peel; Biochar; Adsorption; Ammonium.

1. Introduction

Water eutrophication has become a major environmental problem worldwide to cause the destruction of aquatic ecosystems and degradation of the self-purification capacity of water (Qianqian Yin, 2017). Ammonium (NH_4^+), which is the most common form of nitrogen(N), accounts for a large proportion of soluble nitrogen in wastewater and often results in water eutrophication (Takaya et al., 2016; Tang et al., 2019). It is therefore necessary to remove ammonium from water to maintain a healthy aquatic ecosystem (Xu et al., 2019). To date, several technologies have been devised and implemented to remove NH_4^+ from eutrophic waters (Huang et al., 2017; Provolo et al., 2017; Zhang et al., 2016). For example, the biological process for the removal of ammonium is sensitive to operational parameters, and the running costs are expensive (He et al., 2017). Chemical technology for ammonium removal mainly depends on precipitation, which may cause additional pollution (Yang et al., 2018). Physical methods, especially adsorption, are superior to other approaches because of the economic and environmentally friendly features. These methods are considered to be an economic and effective strategy for removing ammonium (Luo et al., 2019; Vu et al., 2017). Various adsorbents have been used to remove contaminants from wastewater, such as activated carbon (Mochizuki et al., 2016), zeolite (He et al., 2019), and ion exchange resin (Muhammad et al., 2019). However, these materials have some limitations of use due to the high consumption of energy and poor efficiency. In recent decades, biochar has been widely used in the removal of contaminants from wastewater

because of their high efficiency and low cost (Vikrant et al., 2018).

Biochar is a solid by-product derived from the thermochemical conversion of low-cost biomass under oxygen-limited conditions. Due to its negative surface charge, charge density, high degree of porosity, and extensive surface area, biochar has been considered as a low-cost material with sufficient suitability and selectivity (Wang et al., 2018). It can be used in soil improvement, waste management, mitigation of climate change and the environment (Ruan et al., 2019). Biochar has a wide range of biomass sources, including crop residues, forestry wastes, kitchen waste, animal manures and other materials (Luo et al., 2019). Application of biochar to remove inorganic nitrogen (NH_4^+、NO_2^-、NH_3、NO、NO_2、N_2O) from wastewater and agricultural fields has gained a significant interest. The mechanism of inorganic nitrogen interactions with biochar through the known chemisorptions mechanisms, including electrostatic interaction, surface complexation with oxygen-containing functional groups, hydrophobic and hydrophilic interaction etc.(Cui et al., 2016; Sumaraj and Padhye, 2017) To date, several studies have explored the adsorption of NH_4^+ using biochar. The biochar derived from the Mg-Al-modified soybean straw had low adsorption capacity (0.7 mg/g) of NH_4^+ (Yin et al., 2018). Biochar produced from the co-pyrolysis of sewage sludge and walnut shell could reach 22.85 mg/g adsorption capacity of NH_4^+ (Yin et al., 2019). Furthermore the biochar derived from rice straw and the NH_4^+-N adsorption capacity was 15.79 mg/g at 300°C(Park et al., 2019). Xu et al., (2019) analyzed biochars derived from different feedstock materials at different pyrolysis temperatures to remove ammonium. The highest NH_4^+ adsorption capacities were associated with biochars of

rice straw (4.20 mg/g) and sawdust (3.30 mg/g) produced at 500℃ and Phragmites communis (3.20 mg/g) and egg shell (2.20 mg/g) at 300℃. According to the literature, the raw materials used for biochar and the preparation conditions are the key factors in determining the adsorption capacity and performance of the actual biochar used.

Fruit peel residue has been identified as an important source of solid waste, which is a huge challenge for municipal waste management (Sial et al., 2019). The traditional treatment for peel residue is disposal to landfill, composting and incineration, which may cause environmental pollution due to the harmful emissions gases (Lam et al., 2018). These peel residues can be converted into biochar by pyrolysis technology, which has attracted greater scientific attention in recent years (Sial et al., 2019). Wang et al., (2016) absorbed Cr(VI) using pineapple-peel-derived biochar, while in another recent more study, Khan et al., (2019)) undertook research involving the uptake of Cu^{2+} and Zn^{2+} from simulated wastewater using muskmelon peel biochar. Biochar derived from fresh dehydrated banana peels showed excellent Pb adsorption performance (Zhou et al., 2017). Previous studies on biochar derived from fruit peel have focused on the removal of heavy metals from wastewater. However, only a few studies have so far focused on biochar derived from fruit peel to remove ammonium.

In this work, three kinds of fruit peel (orange peel (OP), pineapple peel (PAP), and pitaya peel (PTP)) were collected for making the biochars through slow pyrolysis at 300, 400, 500, 600℃for 2 h and 4 h, respectively. It is hypothesized that fruit peel-derived biochars can be used as an alternative to conventional sorbents in water treatment; especially ammonium can form complexes with oxygen-containing

functional groups on the surface of biochar.

This study aimed to: (*i*) characterize physicochemical properties of the biochars;(*ii*)investigate the NH_4^+ adsorption capacity by biochars produced from various kinds of feedstock; (*iii*) evaluate the effect of pH solution and biochar dosage on the adsorption of NH_4^+; and (*iv*) understand the mechanisms for the removal of NH_4^+ from water using biochars.

2. Materials and methods

2.1 Biochar preparation

Feedstocks of OP, PAP and PTP used in this study were obtained from a fruit supermarket located in Tianjin, China. The materials were rinsed with water and air-dried for two days, and dried in a vacuum drying chamber for 24 h at 105℃. They were then ground and sieved into a powder. An appropriate amount of powder was put into a crucible, sealed with aluminum foil paper, and put it in a muffle furnace. The pyrolysis temperatures were controlled at 300, 400, 500, and 600℃ using a heating rate of 5℃/min, with the residence time of 2 h and 4h, respectively. The biochar samples namely OBC300-2，PBC300-2, and PTBC300-2 correspondingly indicated the orange peel, pineapple peel and pitaya peel biochars were obtained through pyrolysis of 300℃ for 2h. Biochar samples were ground and sieved through 100 meshes. Finally, they were stored prior to use.

2.2 Biochar characterization analysis

Ash content was determined by calculating mass loss of the biochar after being heated at 800℃ for 4 h. To measure the pH and electro-conductivity (EC) of biochars,

each biochar was mixed with distilled water at 1:20, and shaken in a constant temperature oscillator for 24h at 150rp/min and 25 ℃. After this, the pH and EC for suspension was measured. The elemental compositions of C,H,N were conducted using a CHN Elemental Analyzer (Vario ELcube,Germany) while the oxygen content was determined by a mass balance. The surface area and porosity of the biochars were determined by the Brunauer-Emmett-Teller (BET) method with N_2 adsorption isotherms at 77K. Zeta-potential was measured with a potential analyzer (Nano-ZS, United Kingdom). X-ray photoelectron spectrometry (XPS) (K-alpha, United States of America) was used to analyze changes in the surface composition of biochar. The surface functional groups of biochars were analyzed by the Fourier transform infrared (FTIR) system (Nicolet iS10,United States of America),which was conducted in the 400 and 4000 cm^{-1} region with 32 scans being taken at 4 cm^{-1} resolution for identification purposes. Surface morphology of biochar was determined by Scanning electron microscopy (SEM), using the JSM-7800F (Japan). Surface element analysis was conducted simultaneously with the SEM at the same surface locations using energy dispersive X-ray spectroscopy. Thermogravimetric analysis (TGA, STA449F3, Germany) was also undertaken.

2.3 Preliminary evaluation of ammonium adsorption

Adsorption of ammonium by three types of biochars (OP, PAP and PTP) was measured to determine the impact of the pyrolysis parameters on biochar ammonium adsorption capacity. The biochar sample (0.1g) was mixed with 10 mL NH_4^+-N solutions (10 to 100mg/L) in a 50mL centrifugal tube, then placed it in an oscillator at

150 rpm at 25℃. After being shaken for 24h, the mixed liquid was filtered through a 0.45-μm microporous membrane. The concentrations of NH_4^+-N were determined using a UV spectrophotometer (UV-2600, China).The ammonium removal efficiency and ammonium adsorption capacity of different biochar samples were calculated using the following equations. The ammonium removal efficiency is expressed as:

$$R_e(\%)=\frac{C_0-C_e}{C_0}\times 100\% \qquad (1)$$

where, R_e is the ammonium removal efficiency, C_0 is the initial ammonium concentration (mg/L) in the solution, and C_e is the ammonium concentration when at adsorption equilibrium. The ammonium adsorption capacity was calculated as follows:

$$Q_e=\frac{(C_0-C_e)\times V}{m} \qquad (2)$$

where, Q_e is the amount of ammonium adsorbed per unit weight of biochar (mg/g) at equilibrium, V is the volume (L) of the ammonium solution, and m is the mass (g) of the biochar.

2.4 Batch experiments of ammonium adsorption

Based on the preliminary results, OBC300-2, PBC300-2 and PTBC400-2 were selected as the best biochars for ammonium removal. Batch adsorption experiments were carried out as follows. Ammonium stock solutions (1000mg/L) were prepared by dissolving ammonium chloride in ultrapure water. The biochar sample (0.1g) was mixed with 10 mL NH_4^+ solutions (40mg/L) in a 50mL centrifugal tube, under the same conditions as above. Samples were collected at 5, 10, 15, 30, 60, 120, 240, 480,720, 960, 1200, 1440, 2880, and 4320 min and filtered. Sorption isotherms of ammonium were conducted under the same conditions above, and the concentration of NH_4^+ varied

from 10 to 100mg/L (10, 20, 40, 60, 80, 100mg/L). After being shaken for 24h, the mixed liquids were filtered. To investigate the effect of solution pH on ammonium adsorption by biochars, 0.1 g biochars were mixed with 10 mL NH_4^+ solutions (40mg/L). The initial pH of solution was adjusted to 3, 5, 7, 9, 11 using HCl and NaOH. The effect of the dosages (i.e. 0.1, 0.2, 0.5, 1, 2, 3 and 5 g) on the adsorption of NH_4^+-N was evaluated with 10 mL NH_4^+ solutions (40mg/L), and the initial pH of the solution was adjusted to 9 (optimum pH).

2.5 Adsorption kinetics and isotherms

2.5.1 Kinetic models

Adsorption kinetics is usually employed to estimate the adsorption rate, which is critically important for characterizing the adsorption performance of adsorbents. The adsorption kinetics experimental result were fitted to two typical kinetic models:

Pseudo-first-order $q_t = q_e(1 - e^{-k_1 t})$ (3)

Pseudo-second –order $q_t = \frac{k_2 q_e^2 t}{(1+k_2 q_e t)}$ (4)

where, q_e and q_t (mg/g) are the amounts of NH_4^+-N adsorbed by the biochar at the equilibriumand at time t, respectively; k_1 (min^{-1}), and k_2 ($g.mg^{-1}.min^{-1}$) are the rate constants of the pseudo-first-order and pseudo-second –order scenarios.

2.5.2 Adsorption isotherms

To further explore the adsorption mechanism of biochar, the experimental data were fitted to the Langmuir andFreundlich adsorption isotherm models:

Langmuir equation: $Q_e = \frac{C_e Q_m}{(K_L + C_e)}$ (5)

where, Q_m (mg/g) is the maximum absorption capacity; Q_e (mg/g)and C_e (mg/L) are the amounts of adsorbed $NH_4^+$and the NH_4^+ concentrations in the solution at

equilibrium, respectively；and K_L represents the Langmuir constant.

The basic characteristics of the Langmuir isotherm can be expressed by a dimensionless constant known as separation factor R_L. It is usually utilized to evaluate whether the biochar can effectively adsorb NH_4^+. The formula is as follows:

$$R_L = \frac{1}{(1+C_0K_L)} \quad (6)$$

where, K_L is the Langmuir constant and C_0 is the initial concentration of solution (mg/L). R_L represents the effect of initial concentration of solution on the adsorption. The value of R_L indicates the type of isotherm. $0<R_L<1$ is effective adsorption, $R_L>1$represents disadvantageous adsorption, $R_L=1$ is linear adsorption, and $R_L=0$ refers toirreversible adsorption (Jiang et al., 2019).

Freundlich equation: $Q_e = K_F C_e^{1/n}$ (7)

where, K_F represents the Freundlich constant and 1/n is the intensity of adsorption or affinity. The values of 1/n at the range $0<1/n<1$ indicates sorption is indeed favorable. Statistical analysis of the kinetics and sorption isotherms were fitted using Origin Pro 8.0.

3. **Results and discussion**

3.1 Preliminary evaluation of ammonium adsorption

In the preliminary test, the biochars effectively removed ammonium from aqueous solution (Fig.1). Of all three biochars, lower pyrolysis temperature demonstrated superior adsorption ability. Similar results have been documented in other studies in the last few years (Liu et al., 2016; Takaya et al., 2016). It has been shown that pyrolysis time has only a slight effect on biochar's ammonium adsorption. With a comprehensive

consideration of economic viability and benefit, the pyrolysis time is 2 h. OP and PAP biochars had the best adsorption capacity at 300℃, while PTP biochar functioned well at 400℃. This may be related to the raw materials of biochar. OBC300-2, PBC300-2 and PTBC400-2 revealed the best adsorption capacity and consequently they were selected for the following adsorption experiments. All experiments were done in triplicate.

3.2 Characteristics of the biochars

3.2.1 Physicochemical properties

The physicochemical properties of biochars prepared under different pyrolysis conditions are presented in Tables 1 and 2. Tables 1 and 2 showed that pyrolysis temperature exerted a greater effect on the properties of biochar than pyrolysis time. The effect of pyrolysis time on biochars mainly depends on pyrolysis temperature (Zhang et al., 2015). The yield of biochars declined as the temperature increased, which is closely linked to water and volatile organic compounds during the pyrolysis (Wang et al., 2019). Biochars prepared at high temperature had a higher pH value, which may be due to the degradation of acidic functional groups such as carboxylic acids and phenols in biomass. This is accompanied by an increase in carbonization temperature, and is related to the formation of ash and mineral salts (Kwak et al., 2019). Increasing pyrolysis temperature increases EC of biochars, which is due to the decomposition of organic matter (Kwak et al., 2019). Zeta-potentials of the studied biochars were negative (Table 1), indicating that the biochar particles carried negative charges on their surfaces (Wu et al., 2019).

As can be seen in Table 1, the ash content of biochars increased with increasing temperature. This is mainly due to the formation of minerals during pyrolysis (Xu et al., 2019). Obviously, with the increase of pyrolysis temperature and the extension of pyrolysis time, the carbon content of the OBC and PBC biochars increased, while the hydrogen and oxygen content decreased. This was attributed to the increase of temperature, and H and O sing from the carbon chain to form carbon dioxide, water and other new substances which are separate from the carbon body. The result of this was: firstly, the accumulation of C in biochar; and secondly, the gradual decrease of hydrogen and oxygen (Kwak et al., 2019). However, the content of C in PTBC reduced with an increase in temperature, which was possibly due to the high ash content. The results were similar to the report of Xu et al., 2019, who pointed out the content of C in egg shell biochar decreased with an increase in temperature.

Atomic ratio H/C reflects the aromaticity of biochar. The smaller the value, the stronger the aromaticity and the more stable the structure of biochar is. The values of O/C, (O+N)/C represent the level of hydrophilicity and polarity, respectively. The larger atomic ratio exhibited a stronger degree of hydrophilicity and polarity (Chen et al., 2016). H/C, O/C and (O+N)/C decreased with increasing pyrolysis temperature and residence time, which confirmed that the pyrolysis of three fruit peel biochars was a process of aromaticity enhancement, hydrophilicity and polarity reduction. As discovered in this study, the aromaticity order of biochars was PBC>PTBC>OBC, the hydrophilicity order of the biochars was OBC≈PBC>PTBC, and the polarity order of the biochars was OBC≈PBC>PTBC. The OBC300-2 had the highest H/C(0.09),

indicating more organic carbon in biochar cannot be carbonized, which in turn will provide more adsorption sites for inorganic pollutants (Jiang et al., 2019). The OBC300-2 and PBC300-2 had a higher O/C ratio than the other biochars, which caused more oxygen-containing functional groups and surface hydrophilicity.

All these scenarios indicated that the adsorption efficiency of biochar on ammonium is better at low temperature. The specific surface area of biochars increased with increasing temperature. As well, the surface area of three peel biochars from high to low was in turn PTBC, PBC and OBC. However, PTBC had poorer adsorption capacity, which indicates that surface area was not the main factor affecting ammonium adsorption.

3.2.2 Thermogravimetric analysis(TGA) and surface morphology

Thermogravimetric analyses of three raw materials were conducted (supplementary - Fig. S1). The thermal decomposition of the three peels was similar, which can be divided into three stages. The first stage occurred below 200℃, while dehydration and volatilization of volatile substances occurred mainly at this stage. The second stage had the largest proportion of weight loss, which was the most important stage in the pyrolysis process, where the main events were the decomposition of cellulose, hemicellulose and lignin. At this stage, the weight losses of OP, PAP and PTP were 87.59%, 90.2% and 71.56%, respectively. The last phase was the final carbonization stage, and the weight loss curve tends to be flat, indicating that the pyrolysis of cellulose and hemicellulose was basically completed (Novais et al., 2018). Scanning electron microscopy (SEM) of three fruit eels at different temperatures for 2h

are illustrated in Supplementary data - Fig. S3.The biochars were smooth and some stomata were not obvious at 300 ℃. With the increase in temperature, pores gradually appeared on the surface of biochar, and the stomata appeared to develop well and have a well-developed tubular structure. There were significant differences in surface morphology among the biochas derived from different fruit peel species. From the micromorphology of OBC, PBC and PTBC, it can be see that OBC and PBC with the fine macropor (>50nm) developed well, as compared to PTBC. As is shown in Table2, the pore diameter of all samples is in the mesoporous range (2-50nm).

As OBC300-2, PBC300-2 and PTBC400-2 had a higher adsorption capacity, so they were used to investigate the morphological structures and elemental composition (Fig. S2). The EDS spectrum demonstrated that the C, O, K elements dominated the surface of biochars, with Mg, P, S, K, Ca present at different proportions. The surface oxygen content of OBC300-2 (71.86%) and PBC300-2 (71.45%) were higher than that of PTBC400-2(67.22). The higher content of K and Ca in PTBC400-2 results in higher ash content and pH value of biochar, which is in accordance with the results of element analysis (Table 2).

3.2.3 Functional groups analysis

The surface of biochar contains a large number of functional groups (Fig.2), which are beneficial to the adsorption by biochar. In the previous analysis, the band around 3400cm^{-1} represented the stretching vibration of hydroxyl groups (Zhang et al., 2019). Results showed that the intensity of -OH stretching of biochars decreasedwith an increase in temperature, illustrating a large number of hydroxyl groups were

decomposed during the pyrolysis of three biochars.The peaks at 2916-2852cm^{-1}corresponded to the–CH_2 groups (Li et al., 2019c). However, this peak disappeared at higher temperatures, suggesting that most aliphatic compounds converted to carbon dioxide, methane and other gases with the rise in temperature. Furthermore, the peaks at 1640-1390cm^{-1} corresponded to C=O(C-O) stretching vibration of the carboxyl groups (Cui et al., 2016). At higher temperatures, the strength of the functional groups at the peak gradually declined. The strong peak at 1056cm^{-1} was associated with the bond for C-O-C aliphatic/ether stretching(Li et al., 2019a).The peak at 670cm^{-1} represented the aromatic C-H vibration. The functional groups of biochars were abundant at low temperature (Figure 2). With the increase in temperature, the functional groups gradually weakened and partly disappeared, which proved that biochar had better adsorption at low temperature.

3.3 Adsorption kinetics and isotherms

3.3.1 Adsorption kinetics

The adsorption kinetics of OBC300-2, PBC300-2 and PTBC400-2 were shown in the Fig.3(a). At the initial stage of adsorption (0-120min), the adsorption capacities of the biochars for NH_4^+ increased rapidly with time. Subsequently, it changed slowly over a period of time (120-720min). After 720 minutes, the adsorption capacity of NH_4^+ on biochars tended to be balanced. The adsorption experimental data fitted the pseudo-second-order kinetic model with the high R^2 (Table 3). The square correlation coefficients of OBC300-2, PBC3000-2 and PTBC400-2 were 0.99, 0.99 and 0.98, respectively. Experimental results showed that the pseudo-second-order kinetic model

can be used to predict the adsorption kinetics of ammonium (Tang et al., 2019), indicating that the adsorption of ammonium by biochar is a chemical reaction, such as precipitation, complexation and ion exchange (Xu et al., 2019).

3.3.2 Adsorption isotherms

The adsorption isotherms of ammonium on OBC300-2, PBC300-2 and PTBC400-2 biochars can be described by the Langmuir and Freundlich models (Fig. 3(b)). The Langmuir model is based on the assumption that the adsorption occurs in a complete monolayer on a homogenous surface. Meanwhile, the Freundlich isotherm serves to describe heterogeneous systems and reversible adsorption (Tang et al., 2019). As shown in Table 4, among the three biochars, PBC300-2 exhibited the highest theoretical adsorption capacity. The Langmuir model fitted the experimental data better than the Freundlich model with higher correlation coefficients (R^2). The square correlation coefficients of OBC300-2, PBC3000-2 and PTBC400-2 were 0.96, 0.99 and 0.99, respectively. This demonstrated that the surface of biochar was homogeneous and ammonium adsorbed on the surface with similar binding energy. The separation factor R_L of OBC300-2，PBC300-2 and PTBC400-2 was respectively in the 0.11-0.57,0.25-0.77 and 0.10-0.55 range, indicating that ammonium sorption on the biochars was favorable (Li et al., 2019b).

Among the biochars, the maximum theoretical adsorption capacity of OBC300-2, PBC300-2 and PTBC400-2 for ammonium were 4.71, 5.60 and 2.65 mg/g, respectively. The adsorption capacity of biochar to ammonium is in turn: PBC300-2>OBC300-2>PTBC400-2, which suggested that the adsorption of ammonium on biochar was

affected by raw materials. Hale et al., (2013) reported the NH_4^+-N on cacao shell and corn cob biochars were 0.24mg/g and 0.56mg/g, respectively. Recently, Tang et al., (2019) reported that the maximum adsorption capacity of digested sludge biochar to ammonium was 1.40 mg/g. However, the maximum adsorption capacities of wood and rice husk biochars for ammonium were 44.64 mg/g and 39.8 mg/g, respectively (Kizito et al., 2015). Compared to this, fruit peel derived biochars had a moderate sorption capacity for NH_4^+-N.

Obviously, the adsorption capacities of OBC300-2 and PBC300-2 were better than PTBC400-2. The maximum adsorption capacity of PBC300-2 was nearly twice that of PTBC400-2. According to (Cui et al., 2016) and (Xu et al., 2019), biochar with high H/C content is more beneficial to the adsorption of inorganic pollutants. Also, high O/C and (O+N)/C values represent high hydrophilicity and polarity of biochar, which is conducive to the adsorption of polar soluble pollutants such as ammonium. Table 2 shows that OBC and PBC had higher O/C and (O+N)/C than PTBC. The oxygen contents of OBC and PBC were higher than that of PTBC. This means OBC and PBC contained more oxygen-containing functional groups to lead to better ammonium adsorption. The ash content in PTBC was obviously higher than that in OBC and PBC, which was not favorable to ammonium adsorption (Takaya et al., 2016). Compared with PTBC400-2, the surface of OBC300-2 and PBC300-2 has higher polarity and hydrophilicity, and rich oxygen functional groups are more beneficial to the adsorption of ammonium.

3.3.3 Effect of pH on NH_4^+-N removal

The pH value of the solution is one of the most important parameters for optimizing the adsorption process. It mainly affects the adsorption in two ways: (*i*) affecting the surface charge of biochar; and (*ii*) affecting the degree of ionization and existing form of the adsorbate (Tan et al., 2015). In this study, the effect of pH value on the adsorption of ammonium by biochars was shown in Fig. 4. It can be seen from Fig. 4 that the adsorption capacity of ammonium by biochars was lower at lower pH (e.g. pH=3 or 4). With the increase of initial solution pH, the adsorption capacity of ammonium by biochars increased first and then decreased. The adsorption capacity of biochar began to decrease when pH was higher than 9. The results found in this work were similar to those of previous studies. Kizito et al., (2015) showed that the adsorption efficiency was poor at low pH. The adsorption capacity increased when 4<pH <8; however, at pH >8 the adsorption capacity began to decrease at pH >8.

The influence of solution pH on adsorption was mainly attributed to the following three aspects. Firstly, at low pH, some functional groups on the surface of biochar, such as - COOH and - OH, showed positive charges due to protonation which repelled the polar attraction of NH_4^+ ions in aqueous solution (Gong et al., 2019). Secondly, at low pH there was a large amount of H^+ in the solution, which may compete with NH_4^+ for adsorption (Tang et al., 2019; Vu et al., 2017). Thirdly, at high pH, most of $NH_4^+$was converted into NH_3 which cannot be adsorbed on the adsorbent. At this time, electrostatic adsorption is no longer the main mechanism, and adsorption begins to decline (Hou et al., 2016; Tang et al., 2019).

3.3.4 Effect of biochar dosage on NH_4^+-N adsorption

The effect of biochar dosage on adsorption is depicted in Fig. 5.From this figure, the removal efficiency of OBC300-2 increased from 45.83% to 92% while the removal efficiency of PBC300-2 increased from 32% to 91% in the 0.1g-2g range. When the biochar dosage was more than 2g, the removal efficiency of OBC300-2 tended to be stable, and the removal rate of PBC300-2 continued to rise slowly with the removal efficiency reaching 99%. However, the removal efficiency of PTBC400-2 increased from 21.25% to 63.33% in the 0.1-3g range. When biochar dosage was more than 3g, the removal efficiency started reducing. The adsorption capacity of biochars decreased with an increase in the dosage. The results proved to be similar to those reported in other studies (Divband Hafshejani et al., 2016). The reason for this phenomenon was that in the initial stage, with the increase in the amount of adsorbent, the surface area of biochar and the adsorption sites increased. If the dosage of adsorbent continues to increase, there will then be an overlap in the adsorbent layer, and the active sites available on adsorbent will be shielded (Kizito et al., 2015).

3.4 Possible mechanisms for NH_4^+-N adsorption on biochars

To explore the potential mechanism of ammonium adsorption by biochar, the surface functional groups of biochar before and after adsorption were analyzed (supplementary data- Fig. S4). Obviously, the peaks for the three kinds of biochars at 3400 cm^{-1} around (-OH) and 1400 cm^{-1} around (C=O) weakened after ammonium adsorption. It was assumed that these functional groups participated in ammonium adsorption through surface complexation (Cui et al., 2016). On the other hand, these functional groups (- COOH, - OH) are negatively charged and adsorb ammonium by

electrostatic interaction. Hence, better ammonium adsorption capacity can be obtained at low temperature due to the existence of more negative charged functional groups (Sumaraj and Padhye, 2017).

The xps spectra of OBC300-2, PBC300-2 and PTBC400-2 before and after the ammonium adsorption were employed to quantify the different C and O forms present on the surface (Supplementary data-Fig S5). Based on previous research results, the $C1_S$ peaks were split into four components. At 284.8 eV (C-(C, H) and (C=C), 286.5 eV(C-(O, N), such as alcohols, amines, or amides, 287.9eV (C=O, O-C-O), such as hemiacetals, acetals, amides, and carboxylates, 289.0eV (O-C=O), like carboxyl or ester functionalities etc(Jin et al., 2018). Similarly, the $O1_S$ peak was de-convoluted into four components. At 531.2eV (O=C), amides, esters, and carboxyl moieties etc, at 532.6eV (C-O-C，C-OH)，alcohols and ethers, at 531.8 and 533.4 eV (O=C-O-(C. H)), ester and carboxyl functionalities(Huang et al., 2018). As shown in Fig S5, the main forms of C on the surface of three biochars are C-(C, H), C=C; the main forms of O are C-O-C, C-OH and O=C=O-(C, H). The quantities of C=O,C-O-C at 287.9eV and C-O-C, C-OH, C-OH at 532.6eV; O=C-O-(C,H) 533.4eV decreased after adsorption, indicating that these functional groups may be involved in the adsorption of ammonium.

Another potential mechanism of ammonium adsorption by biochar wasion exchange. Previous studies have shown that the adsorption of ammonium by biochar is related to CEC, which represents the negative charge on the surface of biochar and is positively correlated with O/C(Hale et al., 2013). From Table 2, OBC and PBC had higher O/C than PTBC, causing the higher adsorption capacity to occur. The

experimental results were similar to those used in previous studies. For example, Cui et al., (2016)studied the adsorption of ammonium by different wetland plants, where by the C.indica derived biochar had the largest sorption capacity for NH_4^+-N due to having higher molar O/C.

Electrostatic attraction was also one of the biochar-derived mechanisms of ammonium adsorption. In this study, the surface zero charges (pH_{pzc}) of OBC300-2, PBC300-2 and PTBC400-2 were 3.9, 4.3 and 3.7, respectively. If the pH of the solution was less than pH_{pzc}, the surface of biochar was positively charged. Conversely, the surface of biochar was negatively charged and NH_4^+ was adsorbed by electrostatic attraction (Sumaraj and Padhye, 2017).

3.5 Environmental significance

Fruits such as orange are largely consumed in the world which generates a significant amount of fruit peel wastes. This type of municipal solid waste is being generated at a rate of approximately 1.3million tons per year. At present, the fruit peels are usually disposed by open burning, landfining and composting, causing various environment issues. For instance, the release of unpleasant odour, and liberation of greenhouse gases (eg. CH_4 and CO_2), and discharge of toxic compounds could cause some acute health effects. In this study, the peel waste was converted into biochar for use as adsorbent to remove ammonium from aqueous solution, which shows advantages over traditional landfill approaches in disposing this waste. Thus, it is an economically and environmentally friendly method.

4. Conclusions

The physicochemical properties of biochars were affected by the type of feedstock and pyrolysis conditions. Biochar from OP and PAP showed better adsorption capacity than PTP. Pseudo-second-order kinetics and the Langmuir model can well describe the adsorption kinetics and isotherm of ammonium on three kinds of biochars. It is evident that low or high pH of the solution is not conducive to the adsorption by biochar. Adsorption of ammonium by biochar mainly depends on complexation, cation exchange and electrostatic attraction. This study shows that fruit peel biochar has the potential to be an effective adsorbent for ammonium removal from water. The exhausted adsorbents containing high ammonium can be used as soil conditioners. Considering the complexity of the actual water environment and the regeneration of adsorbents, further studies on desorption and competitive adsorption (such as heavy metal, organic matter, and other ions) are necessary.

Acknowledgments

The work was supported by Tianjin Municipal Science and TechnologyBureau (No. 18PTZWHZ00140). The authors are also grateful for the support of theJoint Research Centre for Protective Infrastructure Technology and Environmental Green Bioprocess, School of Environmental and Municipal Engineering, Tianjin Chengjian University, Tianjin 300384 and School of Civil and Environmental Engineering, University of Technology Sydney, NSW 2007, Australia.

References

Chen D, Yu X, Song C, Pang X, Huang J, Li Y. Effect of pyrolysis temperature on the chemical oxidation stability of bamboo biochar. Bioresour Technol 2016; 218: 1303-6.

Cui X, Hao H, Zhang C, He Z, Yang X. Capacity and mechanisms of ammonium and cadmium sorption on different wetland-plant derived biochars. Sci .Total Environ 2016; 539: 566-575.

Divband Hafshejani L, Hooshmand A, Naseri AA, Mohammadi AS, Abbasi F, Bhatnagar A. Removal of nitrate from aqueous solution by modified sugarcane bagasse biochar. Ecol. Eng. 2016; 95: 101-111.

Gong H, Tan Z, Zhang L, Huang Q. Preparation of biochar with high absorbability and its nutrient adsorption–desorption behaviour. Sci .Total Environ 2019; 694.

Hale SE, Alling V, Martinsen V, Mulder J, Breedveld GD, Cornelissen G. The sorption and desorption of phosphate-P, ammonium-N and nitrate-N in cacao shell and corn cob biochars. Chemosphere 2013; 91: 1612-9.

He Q, Zhou J, Song Q, Zhang W, Wang H, Liu L. Elucidation of microbial characterization of aerobic granules in a sequencing batch reactor performing simultaneous nitrification, denitrification and phosphorus removal at varying carbon to phosphorus ratios. Bioresour Technol 2017; 241: 127-133.

He W, Gong H, Fang K, Peng F, Wang K. Revealing the effect of preparation parameters on zeolite adsorption performance for low and medium concentrations of ammonium. J. Environ. Sci. 2019.

Hou J, Huang L, Yang Z, Zhao Y, Deng C, Chen Y, et al. Adsorption of ammonium on biochar prepared from giant reed. Environ Sci Pollut Res 2016; 23: 19107-15.

Huang H, Liu J, Zhang P, Zhang D, Gao F. Investigation on the simultaneous removal of fluoride, ammonia nitrogen and phosphate from semiconductor wastewater using chemical precipitation. Chem. Eng. J. 2017; 307: 696-706.

Huang Z, Hu L, Zhou Q, Guo Y, Tang W, Dai J. Effect of aging on surface chemistry of rice husk-derived biochar. Environ. Prog. Sustain. Energy 2018; 37: 410-417.

Jiang YH, Li AY, Deng H, Ye CH, Wu YQ, Linmu YD, et al. Characteristics of nitrogen and phosphorus adsorption by Mg-loaded biochar from different feedstocks. Bioresour Technol 2019; 276: 183-189.

Jin J, Li S, Peng X, Liu W, Zhang C, Yang Y, et al. HNO3 modified biochars for uranium (VI) removal from aqueous solution. Bioresour Technol 2018; 256: 247-253.

Khan TA, Mukhlif AA, Khan EA. Uptake of Cu2+ and Zn2+ from simulated wastewater using muskmelon peel biochar: Isotherm and kinetic studies. Egyptian Journal of Basic and Applied Sciences 2019; 4: 236-248.

Kizito S, Wu S, Kipkemoi Kirui W, Lei M, Lu Q, Bah H, et al. Evaluation of slow pyrolyzed wood and rice husks biochar for adsorption of ammonium nitrogen from piggery manure anaerobic digestate slurry. Sci. Total Environ 2015; 505:

102-12.

Kwak JH, Islam MS, Wang S, Messele SA, Naeth MA, El-Din MG, et al. Biochar properties and lead(II) adsorption capacity depend on feedstock type, pyrolysis temperature, and steam activation. Chemosphere 2019; 231: 393-404.

Lam SS, Liew RK, Cheng CK, Rasit N, Ooi CK, Ma NL, et al. Pyrolysis production of fruit peel biochar for potential use in treatment of palm oil mill effluent. J Environ Manage 2018; 213: 400-408.

Li H, Xiong J, Xiao T, Long J, Wang Q, Li K, et al. Biochar derived from watermelon rinds as regenerable adsorbent for efficient removal of thallium(I) from wastewater. Process Saf. Environ. Protect. 2019a; 127: 257-266.

Li J, Li B, Huang H, Lv X, Zhao N, Guo G, et al. Removal of phosphate from aqueous solution by dolomite-modified biochar derived from urban dewatered sewage sludge. Sci .Total Environ 2019b.

Li N, Yin M, Tsang DCW, Yang S, Liu J, Li X, et al. Mechanisms of U(VI) removal by biochar derived from Ficus microcarpa aerial root: A comparison between raw and modified biochar. Sci .Total Environ 2019c; 697.

Liu Z, Xue Y, Gao F, Cheng X, Yang K. Removal of ammonium from aqueous solutions using alkali-modified biochars. Chem. Speciation Bioavail. 2016; 28: 26-32.

Luo L, Wang G, Shi G, Zhang M, Zhang J, He J, et al. The characterization of biochars derived from rice straw and swine manure, and their potential and risk in N and P removal from water. J Environ Manage 2019; 245: 1-7.

Mochizuki T, Kubota M, Matsuda H, D'Elia Camacho LF. Adsorption behaviors of ammonia and hydrogen sulfide on activated carbon prepared from petroleum coke by KOH chemical activation. Fuel Process. Technol. 2016; 144: 164-169.

Muhammad A, Soares A, Jefferson B. The impact of background wastewater constituents on the selectivity and capacity of a hybrid ion exchange resin for phosphorus removal from wastewater. Chemosphere 2019; 224: 494-501.

Novais SV, Zenero MDO, Barreto MSC, Montes CR, Cerri CEP. Phosphorus removal from eutrophic water using modified biochar. Sci Total Environ 2018; 633: 825-835.

Park MH, Jeong S, Kim JY. Adsorption of NH_3-N onto rice straw-derived biochar. J Environ Chem Eng 2019; 7.

Provolo G, Perazzolo F, Mattachini G, Finzi A, Naldi E, Riva E. Nitrogen removal from digested slurries using a simplified ammonia stripping technique. Waste Manag 2017; 69: 154-161.

Qianqian Yin RW, Zhenghui Zhao. Application of MgeAl-modified biochar for simultaneous removal of ammonium, nitrate, and phosphate from eutrophic water J. Clean Prod. 2017.

Ruan X, Sun Y, Du W, Tang Y, Liu Q, Zhang Z, et al. Formation, characteristics, and

applications of environmentally persistent free radicals in biochars: A review. Bioresour Technol 2019; 281: 457-468.

Sial TA, Khan MN, Lan Z, Kumbhar F, Ying Z, Zhang J, et al. Contrasting effects of banana peels waste and its biochar on greenhouse gas emissions and soil biochemical properties. Process Saf. Environ. Protect 2019; 122: 366-377.

Sumaraj, Padhye LP. Influence of surface chemistry of carbon materials on their interactions with inorganic nitrogen contaminants in soil and water. Chemosphere 2017; 184: 532-547.

Takaya CA, Fletcher LA, Singh S, Anyikude KU, Ross AB. Phosphate and ammonium sorption capacity of biochar and hydrochar from different wastes. Chemosphere 2016; 145: 518-27.

Tan X, Liu Y, Zeng G, Wang X, Hu X, Gu Y, et al. Application of biochar for the removal of pollutants from aqueous solutions. Chemosphere 2015; 125: 70-85.

Tang Y, Alam MS, Konhauser KO, Alessi DS, Xu S, Tian W, et al. Influence of pyrolysis temperature on production of digested sludge biochar and its application for ammonium removal from municipal wastewater. J. Clean Prod. 2019; 209: 927-936.

Vikrant K, Kim KH, Ok YS, Tsang DCW, Tsang YF, Giri BS, et al. Engineered/designer biochar for the removal of phosphate in water and wastewater. Sci Total Environ 2018; 616-617: 1242-1260.

Vu TM, Trinh VT, Doan DP, Van HT, Nguyen TV, Vigneswaran S, et al. Removing ammonium from water using modified corncob-biochar. Sci Total Environ 2017; 579: 612-619.

Wang C, Gu L, Liu X, Zhang X, Cao L, Hu X. Sorption behavior of Cr(VI) on pineapple-peel-derived biochar and the influence of coexisting pyrene. Int. Biodeterior. Biodegrad. 2016; 111: 78-84.

Wang Q, Wang B, Lee X, Lehmann J, Gao B. Sorption and desorption of Pb(II) to biochar as affected by oxidation and pH. Sci Total Environ 2018; 634: 188-194.

Wang X, Chi Q, Liu X, Wang Y. Influence of pyrolysis temperature on characteristics and environmental risk of heavy metals in pyrolyzed biochar made from hydrothermally treated sewage sludge. Chemosphere 2019; 216: 698-706.

Wu L, Wei C, Zhang S, Wang Y, Kuzyakov Y, Ding X. MgO-modified biochar increases phosphate retention and rice yields in saline-alkaline soil. J. Clean Prod. 2019.

Xu D, Cao J, Li Y, Howard A, Yu K. Effect of pyrolysis temperature on characteristics of biochars derived from different feedstocks: A case study on ammonium adsorption capacity. Waste Manag 2019; 87: 652-660.

Yang Q, Wang X, Luo W, Sun J, Xu Q, Chen F, et al. Effectiveness and mechanisms of phosphate adsorption on iron-modified biochars derived from waste activated sludge. Bioresour Technol 2018; 247: 537-544.

Yin Q, Liu M, Ren H. Biochar produced from the co-pyrolysis of sewage sludge and walnut shell for ammonium and phosphate adsorption from water. J Environ Manage 2019; 249: 109410.

Yin Q, Wang R, Zhao Z. Application of Mg–Al-modified biochar for simultaneous removal of ammonium, nitrate, and phosphate from eutrophic water. J. Clean Prod. 2018; 176: 230-240.

Zhang J, Liu J, Liu R. Effects of pyrolysis temperature and heating time on biochar obtained from the pyrolysis of straw and lignosulfonate. Bioresour Technol 2015; 176: 288-91.

Zhang S, Ji Y, Dang J, Zhao J, Chen S. Magnetic apple pomace biochar: Simple preparation, characterization, and application for enriching Ag(I) in effluents. Sci Total Environ 2019; 668: 115-123.

Zhang X, Yu B, Zhang N, Zhang H, Wang C, Zhang H. Effect of inorganic carbon on nitrogen removal and microbial communities of CANON process in a membrane bioreactor. Bioresour Technol 2016; 202: 113-8.

Zhou N, Chen H, Xi J, Yao D, Zhou Z, Tian Y, et al. Biochars with excellent Pb(II) adsorption property produced from fresh and dehydrated banana peels via hydrothermal carbonization. Bioresour Technol 2017; 232: 204-210.

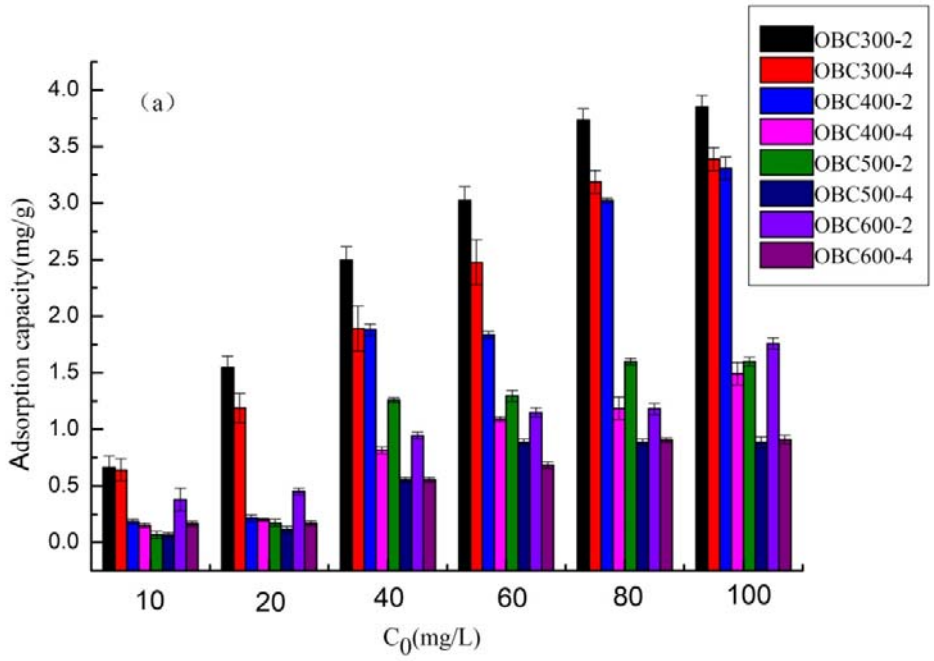
(a)
OBC300-2
OBC300-4
OBC400-2
OBC400-4
OBC500-2
OBC500-4
OBC600-2
OBC600-4
Adsorption capacity(mg/g)
0.0
0.5
1.0
1.5
2.0
2.5
3.0
3.5
4.0
10
20
40
60
80
100
C0(mg/L)

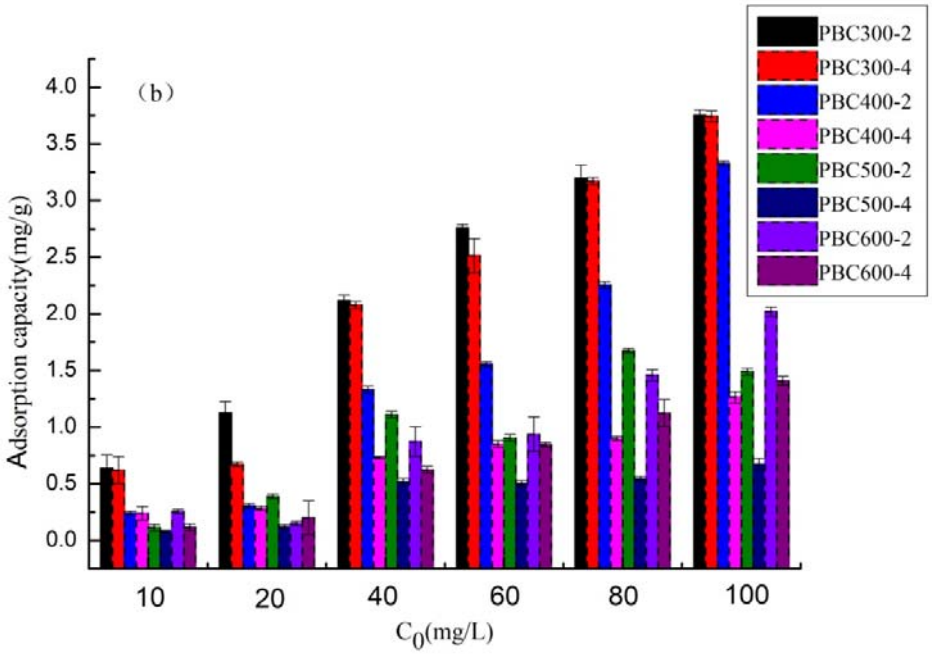
(b)
PBC300-2
PBC300-4
PBC400-2
PBC400-4
PBC500-2
PBC500-4
PBC600-2
PBC600-4
Adsorption capacity(mg/g)
0.0
0.5
1.0
1.5
2.0
2.5
3.0
3.5
4.0
10
20
40
60
80
100
C0(mg/L)

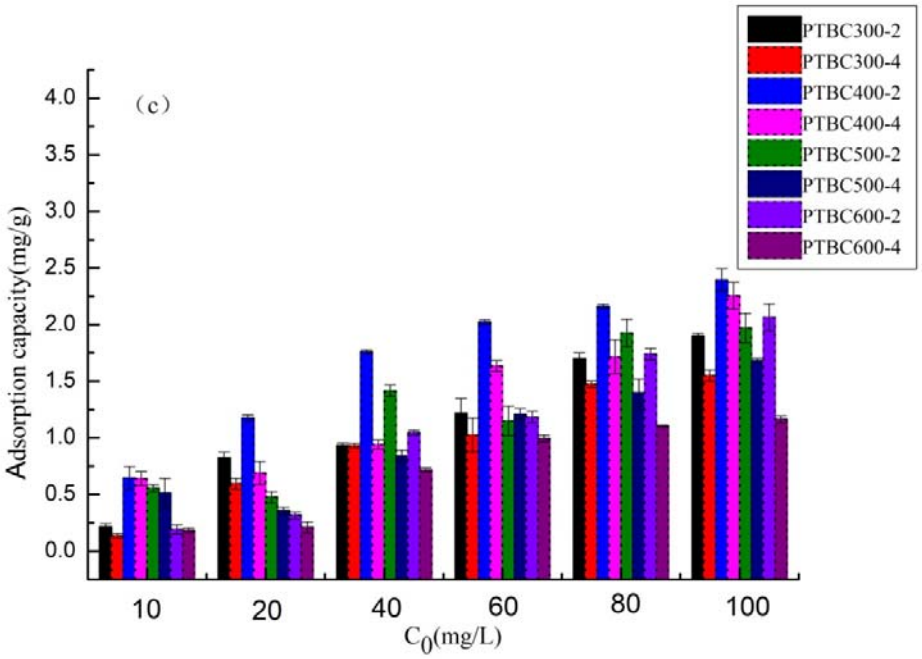

Figure 1. Initial evaluation of ammonium adsorption onto the biochars. (a) biochars derived from orange peel (OBC) at different conditions ; (b) biochars derived from pineapple peel (PAP) at different conditions ; (c) biochars derived from pitaya peel (PTP) at different conditions.

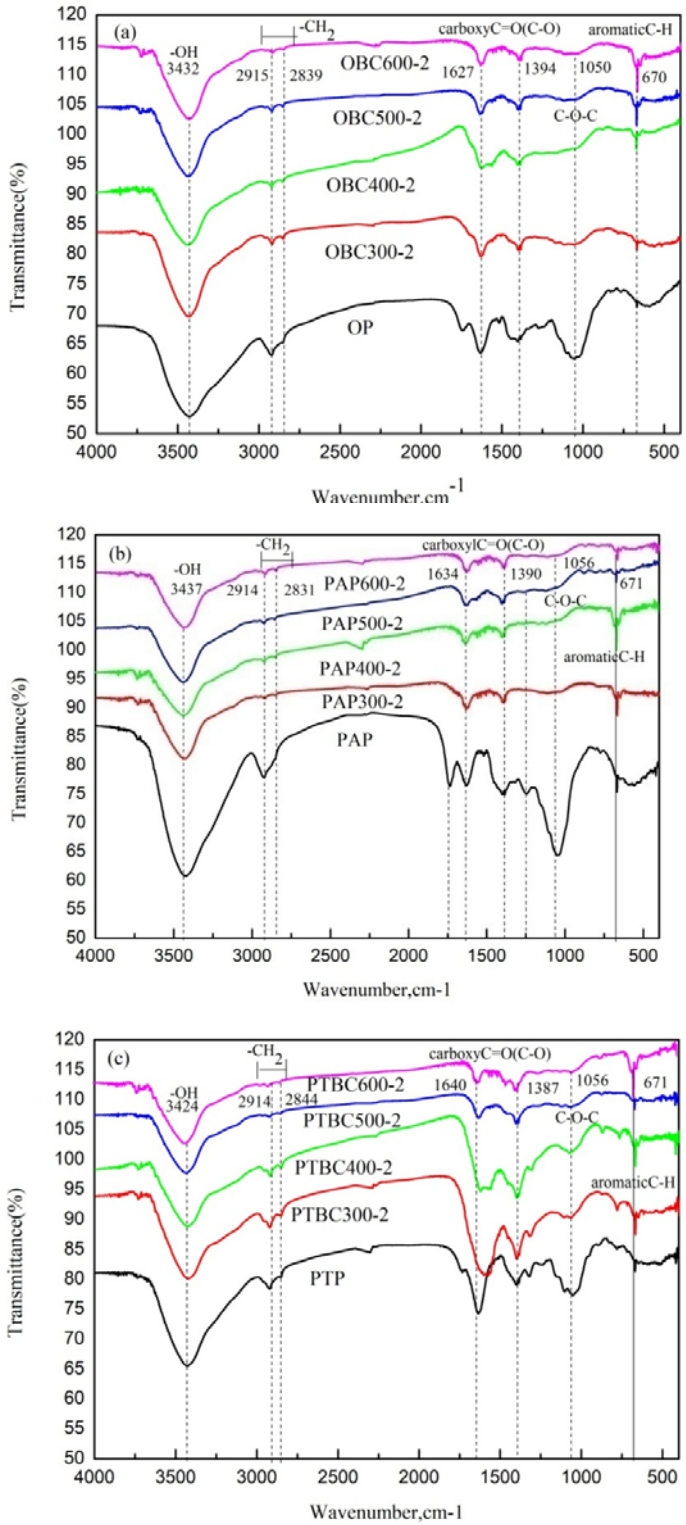

Figure2. Fourier Infrared Images of three fruit peel biochars at different temperatures for 2h. (a) biochars derived from orange peel (OBC); (b) biochars derived from pineapple peel (PAP) ; (c) biochars derived from pitaya peel (PTP).

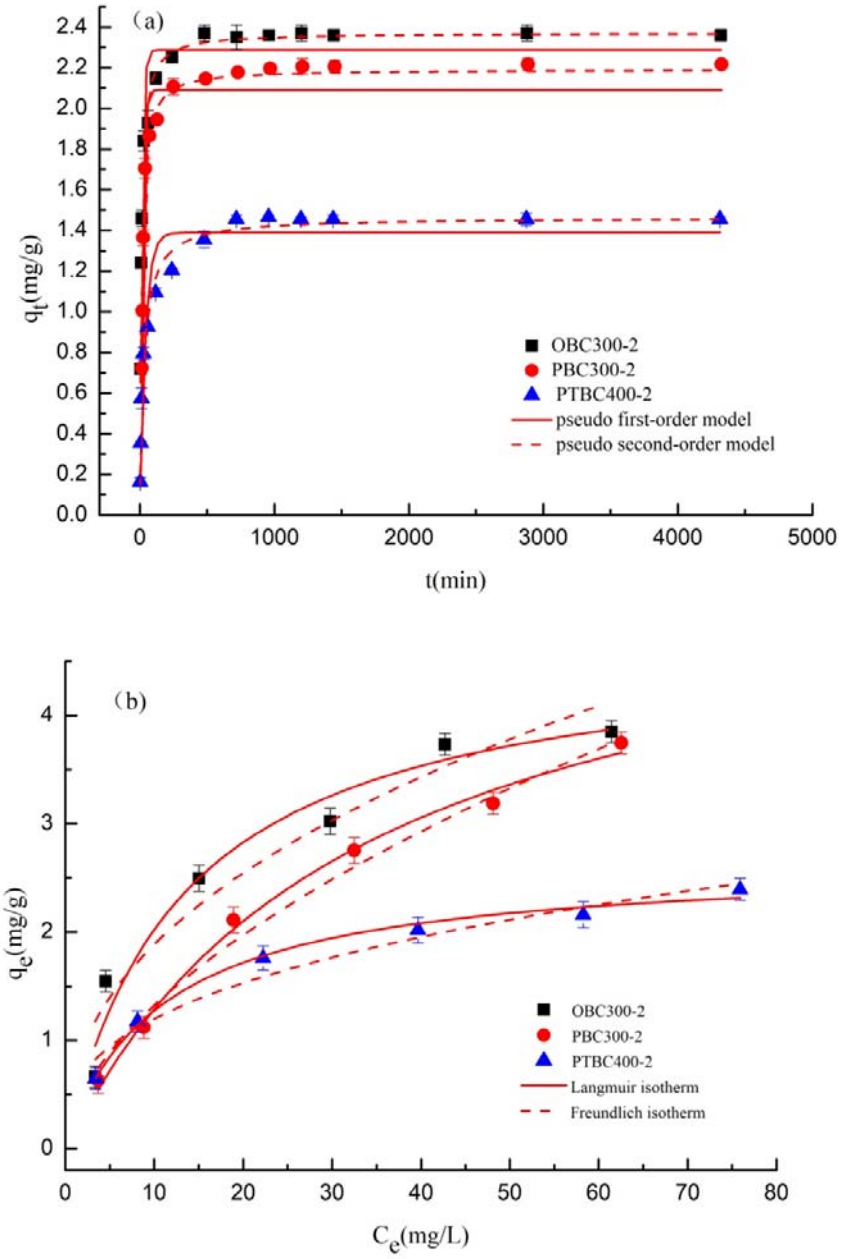

Fig.3 Adsorption kinetics and adsorption isotherm of three best biochars. (a) adsorption kinetics of three best biochars; (b) adsorption isotherm of three best biochars

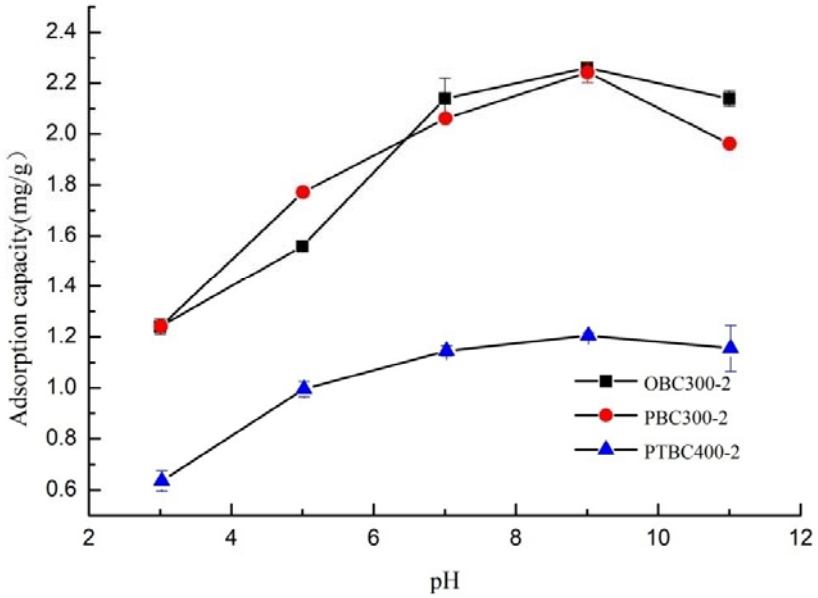

Fig.4 Effect of pH on the adsorption of ammonium by three best biochars

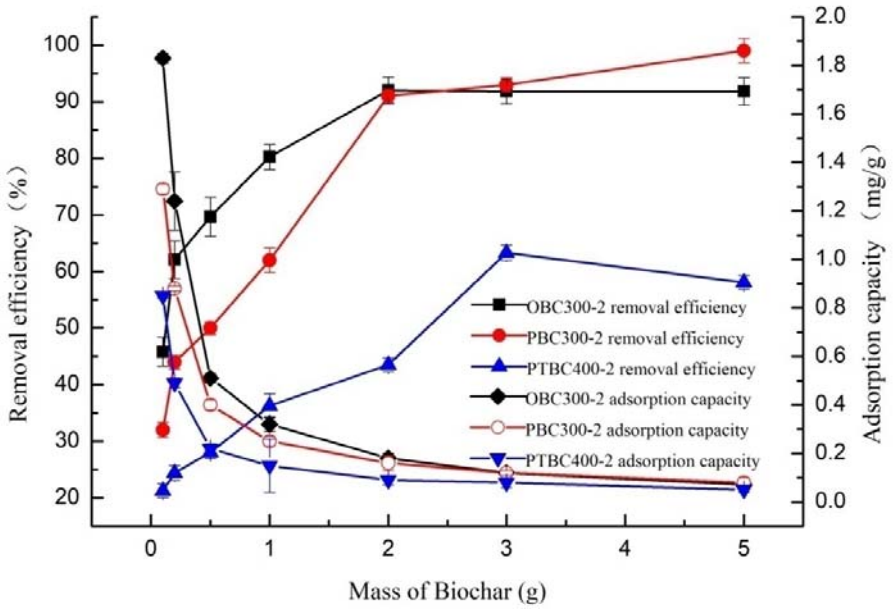

Fig.5 Effect of biochar dosage on the adsorption of ammonium by three best biochars

Table 1
Physicochemical properties of different raw materials and biochars

Sample	Yield(%)	pH	EC(ms/cm)	Zeta potential(mv)
OP	—	4.38±0.00	1.88±0.03	-22.55±0.25
OBC300-2	47.77±0.94	9.60±0.02	1.66±0.02	-48.57±0.29
OBC300-4	44.67±0.47	8.82±0.30	1.31±0.00	-42.17±0.05
OBC400-2	35.20±0.47	10.05±0.03	3.01±0.06	-39.63±0.45
OBC400-4	34.09±0.54	10.31±0.03	2.64±0.02	-35.83±0.45
OBC500-2	30.66±0.14	10.53±0.01	4.13±0.05	-34.00±0.29
OBC500-4	29.33±0.01	10.24±0.00	3.60±0.02	-33.27±0.25
OBC600-2	29.29±0.12	10.58±0.00	5.01±0.08	-33.27±0.26
OBC600-4	25.33±0.02	10.68±0.00	4.93±0.00	-33.40±0.14
PAP	—	3.82±0.10	2.57±0.06	-16.65±0.25
PBC300-2	49.52±0.02	8.65±0.16	2.71±0.05	-48.90±0.24
PBC300-4	49.50±0.50	8.21±0.04	2.36±0.03	-42.30±0.34
PBC400-2	36.80±0,20	10.37±0.04	3.71±0.04	-43.33±0.40
PBC400-4	36.50±0.00	10.02±0.00	3..54±0.02	-42.47±0.19
PBC500-2	34.10±0.10	10.18±0.03	4.53±0.02	-33.67±0.33
PBC500-4	31.62±0.41	10.07±0.01	4.67±0.05	-30.17±0.09
PBC600-2	32.00±0.20	10.47±0.02	5.80±0.02	-30.87±0.56
PBC600-4	28.67±0.01	10.40±0.01	5.66±0.03	-24.63±0.40
PTP	—	4.38±0.04	8.46±0.14	-24.70±0.05
PTBC300-2	50.14±0.14	10.69±0.04	14.58±0.55	-43.53±0.21
PTBC300-4	44.62±0.05	10.76±0.00	14.92±0.04	-37.43±0.33
PTBC400-2	41.14±0.29	11.38±0.02	19.94±0.12	-32.50±0.37
PTBC400-4	40.44±0.25	11.26±0.01	18.56±0.14	-31.50±0.54
PTBC500-2	36.00±0.00	11.52±0.06	23.57±0.31	-31.60±0.37
PTBC500-4	31.34±0.01	11.51±0.01	22.57±0.17	-30.60±0.14
PTBC600-2	33.33±0.00	12.66±0.03	25.13±0.12	-25.33±0.12
PTBC600-4	29.93±0.07	12.41±0.00	25.43±0.09	-17.40±0.24

* OP, PAP and PTP represent orange peel, pineapple peel and pitayapeel,respectively. OBC300-2, OBC300-4, OBC400-2, OBC400-4, OBC500-2, OBC500-4, OBC600-2, OBC600-4 represent orange peel biochar at 300,400,500 and 600℃ for 2h and 4h, respectively. PBC300-2, PBC300-4, PBC400-2, PBC400-4, PBC500-2,PBC500-4, PBC600-2, PBC600-4 represent pineapple peel biochar at 300,400,500 and 600℃ for 2h and 4h, respectively. PTBC300-2, PTBC300-4, PTBC400-2, PTBC400-4, PTBC500-2,PTBC500-4, PTBC600-2, PTBC600-4 represent pineapple peel biochar at 300,400,500 and 600℃ for 2h and 4h, respectively. Date are means ±SD (n=3)

Table 2
Elemental composition and specific surface area of different raw materials and biochars

Sample	Component(%)					Atomic ratio			SA(m^2/g)	TPV(cm^3/g)	PD(nm)
	Ash	C	H	O[a]	N	H/C	O/C	(O+N)/C			
OP	3.18±0.06	47.11±0.01	8.10±0.22	43.59±0.26	1.20±0.05	0.17	0.83	0.95	—	—	—
OBC300-2	6.37±0.12	66.50±0.04	6.05±0.03	19.01±0.08	2.09±0.10	0.09	0.29	0.32	0.55	0.0017	12.2
OBC300-4	6.49±0.04	67.78±0.10	5.25±0.02	18.43±0.06	2.05±0.02	0.08	0.27	0.30	0.62	0.0020	12.7
OBC400-2	8.34±0.19	71.86±0.23	5.01±0.02	12.73±0.18	2.06±0.07	0.07	0.18	0.21	0.63	0.0021	13.3
OBC400-4	8.52±0.08	72.79±0.06	4.65±0.01	11.91±0.09	2.13±0.02	0.06	0.16	0.19	0.67	0.0022	13.1
OBC500-2	10.03±0.18	76.57±0.05	3.08±0.05	8.26±0.11	2.07±0.02	0.04	0.11	0.13	0.70	0.0025	14.2
OBC500-4	10.51±0.04	76.73±0.10	2.92±0.01	7.76±0.13	2.08±0.04	0.04	0.10	0.13	0.75	0.0027	14.3
OBC600-2	10.69±0.17	78.00±0.07	2.27±0.04	7.04±0.10	2.00±0.00	0.03	0.09	0.12	0.92	0.0032	14.0
OBC600-4	10.80±0.16	78.51±0.45	2.03±0.02	6.51±0.46	2.15±0.01	0.03	0.08	0.11	0.92	0.0032	14.0
PAP	3.13±0.05	45.76±0.06	6.50±0.10	47.21±0.22	0.53±0.06	0.14	1.03	1.04	—	—	—
PBC300-2	6.58±0.08	68.57±0.22	4.25±0.05	19.7±0.32	0.90±0.05	0.06	0.29	0.30	0.54	0.0013	9.4
PBC300-4	6.64±0.06	69.11±0.14	3.97±0.00	18.72±0.47	1.56±0.05	0.06	0.27	0.29	0.57	0.0014	9.8
PBC400-2	8.47±0.13	74.50±0.08	3.37±0.08	12.63±0.05	1.03±0.05	0.05	0.17	0.18	0.52	0.0015	11.7
PBC400-4	8.56±0.16	74.82±0.39	3.34±0.03	12.46±0.41	0.82±0.03	0.04	0.17	0.18	0.79	0.0026	13.0
PBC500-2	9.43±0.12	78.04±0.05	2.56±0.02	8.95±0.04	1.03±0.02	0.03	0.11	0.13	0.90	0.0030	13.4
PBC500-4	9.49±0.17	78.43±0.47	2.41±0.37	8.79±0.09	0.89±0.02	0.03	0.11	0.12	0.94	0.0032	13.7
PBC600-2	10.05±0.02	78.84±0.07	1.59±0.07	8.51±0.03	1.01±0.04	0.02	0.11	0.12	1.26	0.0039	12.3
PBC600-4	10.05±0.01	79.08±0.03	1.57±0.36	8.36±0.39	0.95±0.01	0.02	0.11	0.12	1.28	0.0042	13.1
PTP	13.91±0.05	44.45±0.20	5.83±0.40	47.9±0.6	1.82±0.00	0.13	1.08	1.12	—	—	—
PTBC300-2	28.64±0.14	54.25±0.21	4.18±0.04	10.79±0.31	2.15±0.06	0.08	0.20	0.24	1.27	0.0051	16.2
PTBC300-4	29.32±0.07	54.79±0.01	3.86±0.04	10.18±0.09	1.86±0.04	0.07	0.19	0.22	1.38	0.0042	12.1
PTBC400-2	35.84±0.33	50.52±0.02	2.87±0.04	9.07±0.01	1.71±0.02	0.06	0.18	0.21	1.46	0.0073	20.0

PTBC400-4	36.08±0.19	50.69±0.09	2.58±0.03	9.23±0.15	1.43±0.03	0.05	0.18	0.21	1.47	0.0074	20.3
PTBC500-2	41,83±0.57	48.76±0.03	1.64±0.04	6.34±0.07	1.43±0.00	0.03	0.13	0.16	1.52	0.0047	12.4
PTBC500-4	42.33±0.37	48.57±0.13	1.61±0.08	6.48±0.16	1.01±0.05	0.03	0.13	0.15	1.59	0.0059	14.9
PTBC600-2	44.97±0.05	47.32±0.07	1.01±0.00	5.28±0.14	1.42±0.07	0.02	0.11	0.14	1.69	0.0065	15.3
PTBC600-4	46.25±0.02	47.32±0.02	1.04±0.00	4.30±0.07	1.10±0.03	0.02	0.09	0.11	1.67	0.0072	17.4

[a]O content determined by difference.

Table 3

Kinetic parameters of ammonium sorption onto biochars obtained from the pseudo-first-order,pseudo-second-order models

Biochar type	pseudo-first order kinetics		
	$K_1(min^{-1})$	$q_e(mg/g)$	R^2
OBC300-2	0.06707	2.28788	0.93881
PBC300-2	0.06900	2.09512	0.92143
PTBC400-2	0.02394	1.39357	0.93426
	pseudo-second order kinetics		
	K_2(g.mg-1.min-1)	$q_e(mg/g)$	R^2
OBC300-2	0.04239	2.37201	0.99122
PBC300-2	0.04080	2.19606	0.99008
PTBC400-2	0.02276	1.46881	0.98471

Table 4

Sorption parameters of ammonium on the biochars obtained from the Langmuir and Freundlich isotherm model

Biochar type	Langmuir isotherm		
	Q_{max}(mg/g)	K_L(L/mg)	R^2
OBC300-2	4.70905	0.07512	0.95623
PBC300-2	5.59782	0.03025	0.99312
PTBC400-2	2.64683	0.09165	0.99176

	Freundlich isotherm		
	K_F(mg/g(L/mg)$^{1/n}$)	1/n	R^2
OBC300-2	0.6976	0.43194	0.92745
PBC300-2	0.36126	0.56816	0.98600
PTBC400-2	0.52845	0.35395	0.95749